

## A Stochastic Multi-Scale Model for Prediction of the Autogenous Shrinkage Deformations of Early-age Concrete

S. Liu<sup>1</sup>, X. Liu<sup>2,3</sup>, Y. Yuan<sup>2</sup>, P. F. He<sup>1</sup> and H. A. Mang<sup>2,4</sup>

**Abstract:** Autogenous shrinkage is defined as the bulk deformation of a closed, isothermal, cement-based material system, which is not subjected to external forces. It is associated with the hydration process of the cement paste. From the viewpoint of engineering practice, autogenous shrinkage deformations result in an increase of tensile stresses, which may lead to cracking of early-age concrete. Since concrete is a multi-phase composite with different material compositions and microscopic configurations at different scales, autogenous shrinkage does not only depend on the hydration of the cement paste, but also on the mechanical properties of the constituents and of their distribution. In this paper, a stochastic multi-scale model for early-age concrete is presented, which focuses on the prediction of autogenous shrinkage deformations. In this model, concrete is divided into three different levels according to the requirement of separation of scales. These levels are the cement paste, the mortar, and the concrete. A specific representative volume element (RVE) for each scale is described by introducing stochastic parameters. Different scales are linked by means of the asymptotic expansion theory. A set of autogenous shrinkage experiments on the cement paste, the mortar, and the concrete is conducted and used for validation of the developed multi-scale model. Furthermore, the influence of the type and the volume fraction of the aggregate on autogenous shrinkage is studied. Besides, a combined optimum of fine and coarse aggregates is determined. The analysis results show that the proposed model can effectively estimate the autogenous shrinkage deformations of concrete at early-age by taking the influence of the material composition and configuration into consideration.

**Keywords:** Autogenous shrinkage, Early-age concrete, Stochastic multi-scale

---

<sup>1</sup> Institute of Applied Mechanics, Tongji University, Shanghai, China.

<sup>2</sup> Department of Geotechnical Engineering, Tongji University, Shanghai, China.

<sup>3</sup> Corresponding author. Email: Xian.liu@tongji.edu.cn

<sup>4</sup> Institute of Mechanics of Materials and Structures, Vienna University of Technology, Vienna, Austria.

model, Asymptotic expansion method.

## 1 Introduction

In the construction of massive concrete structures, such as dams, immersed tunnels, basements, and wharfs, crack control at early-age has been a very important aspect [Wang (1997); Shen and Xie (2006)]. Cracking of concrete reduces the load-carrying capacity of the structure; moreover, it may also lead to leakage, corrosion, and rupture of the reinforcement. This may reduce the durability of structures and finally cause structural damage. Hence, cracking of concrete has a negative effect on the service life of structures and ultimately on their safety performance [Ye and Tian (2013); Min and Jung (2010)].

In order to satisfy the requirements for High Performance Concrete (HPC), such as low permeability and diffusivity, a low water to binder ratio (w/b) with a large amount of binder is essential. In concrete with  $w/b < 0.5$ , most of the mixed water remains bound to the binder, which causes a reduction of the specific volume of water through chemical absorption during hydration. Small pores in the cement paste gradually develop, and the vapor pressure and the relative humidity decrease accordingly, without supply of water. Closely related to this change of relative humidity, the cement paste undergoes autogenous shrinkage [Lura and Jensen (2003); Li and Bao (2010)]. This results in tensile stresses due to internal restraint from aggregates or external restraint from adjunct elements. When the stresses exceed the tensile strength, micro or macro cracking will occur. [Holt and Leivo (2006); Lura and Jensen (2009); Darquennes, Staquet, Marie and Bernard (2011)].

Quantifying the autogenous shrinkage deformations is a prerequisite to the fundamental understanding of autogenous shrinkage as well as the development of numerical models for stress analysis. So far, the main focus of research on autogenous shrinkage of cementitious materials has been on the mechanism [Tazawa and Miyazawa (1998); Zhang, Hou and Wei (2010)] and on its influence factors. The factors were investigated by means of experiments on the macroscopic scale, considering the type of cement [Lura, Breugel and Maruyama (2001); Zhutosky, Kovler and Bentur (2004)], the aggregates [Kohno, Okamoto, Isikawa and Mori (1999); Idiart, Bisschop, Caballero and Lura (2012)], the admixtures [Lee and Kim (2006); Yoo, Kwon and Jung (2012)], and external environmental factors [Lura, Breugel and Maruyama (2001); Gaurav (2012)]. However, such experimental research activities are usually limited to one particular factor, which is not enough to fully understand autogenous shrinkage.

At present, there are two different ways to measure autogenous deformations of cement-based materials. One is the volumetric deformation method, and the other

one is the one-dimensional deformation method [Wang and Li (2013); Barcelo and Boivin (1999); Bjøntegaard, Hammer and Sellevold (2004)]. For the cement paste and the mortar, the volumetric deformation method is standardized and well applied, because it can be measured from the beginning of the set, and it can be easily operated with high precision. However, for concrete, rigid aggregates may pierce the rubber bag during molding. Hence, the volumetric deformation method cannot be applied. Therefore, the one-dimensional deformation method is chosen. However, so far, there exists no uniform standard test method for autogenous shrinkage of concrete at early-age. Different researchers have designed different experimental devices and methods, based on specific research goals and available laboratory conditions. In tests of autogenous shrinkage, concrete specimens should not only be sealed to prevent moisture exchange with the surrounding environment, but also measured without constraints of the deformations. Besides, since autogenous shrinkage varies strongly at early-age, its measurement should start already at the formation of the initial structure of concrete. Thus, it is difficult to accurately measure autogenous shrinkage deformations of concrete at early-age. On that account, autogenous shrinkage of concrete, as treated in the literature varies enormously, both in magnitude and direction. Therefore, there is not enough confidence in these results, allowing them to be used in engineering practice.

For these reasons, several researchers have developed mechanical models for autogenous shrinkage of concrete by investigating mechanisms based on the material composition, the microscopic configuration, the relative humidity and so on [Liu, Zhao, Deng and Liang (2009); Slowik, Hübner, Schmidt and Villmann (2009)]. Other researchers have fitted data obtained from macroscopic experiments in form of linear functions, exponential functions, power functions or combinations of such functions [ACI Committee (2009); Chu, Kwon, Amin and Kim (2012)]. However, the resulting macroscopic models depend on the available experimental means, i.e. on macroscopic experiments of concrete. Thus, it is understandable that the range of application of macroscopic models of autogenous shrinkage is limited.

The main reasons of the aforementioned problems are that, as a kind of multi-phase composite, concrete consists of cement paste and aggregates. Besides, along with the hydration reaction of cement, its mechanical behavior shows significant time variability. Multi-scale mechanics provides a new approach to treat problems of early-age concrete. It divides concrete into different scales and assumes that it has different compositions and microscopic configurations at different scales and that the individual scales can be linked by means of homogenization strategies [Constantinides and Ulm (2004)]. This approach was chosen by several researchers [Pichler, Lackner and Mang (2007); Kar, Ray, Unnikrishnan and Davalos (2013); Zhang and Hou (2012)], using micro-mechanics of composites. However,

in these models some assumptions were made to simplify the calculation, which does not reflect the random configuration of concrete. Since concrete is a typical non-homogenous composite, autogenous shrinkage of this material does not only depend on the hydration of the cement paste, but also on the mechanical properties of the constituents and of their distribution. In order to take these characteristics into account, multi-inclusion unit cell models have been proposed [Böhm, Han and Eckschlager (2004); Dong and Atluri (2013)], and some recent works of computational grains, which significantly reduces the burden of FEM meshing and computation have been published [Dong and Atluri (2012); Dong and Atluri (2013); Dong and Gamal (2013)]. Asymptotic expansion theory has been proposed as a calculation method [Cui and Cao (1998)] that is suitable for composite materials of periodic or random configuration with a high inclusion content. It takes the interaction between the inclusions into account [Li and Cui (2005); Liu, Liu, Guan, He and Yuan (2013); Yu and Cui (2007)].

In this paper, a stochastic multi-scale model for early-age concrete, focusing on the prediction of autogenous shrinkage deformations, is presented. The scope of the work is outlined as follows: Concrete is divided into three different levels according to the requirement of separation of scales. For each scale, a specific RVE is defined by introducing stochastic parameters, and the asymptotic expansion theory is applied for the development of upscaling schemes. A set of contrasting experiments on autogenous shrinkage with respect to the cement paste, the mortar, and the concrete is conducted and used for validation of the developed model. Besides, the influence of the type and the volume fraction of aggregates on autogenous shrinkage of concrete is investigated.

## **2 Representation**

To predict autogenous shrinkage of concrete more accurately, concrete is divided into three scales below the macro-scale: the concrete scale, the mortar scale, and the cement paste scale, as shown in Fig. 1, according to the requirement of separation of scales.

The cement paste is regarded as isotropic and homogenous. Its mechanical parameters and autogenous shrinkage are obtained through a standardized test, which is highly precise from the beginning of the set.

The mortar is considered as a two-phase composite that consists of cement paste as the matrix and sand as the inclusion. A simple RVE with randomly distributed sand could be insufficient for providing reliable estimates of the properties of mortar. Therefore, a series of specific RVEs are proposed. Each of them is assumed to consist of the matrix and of spherical inclusions, which are non-overlapping and

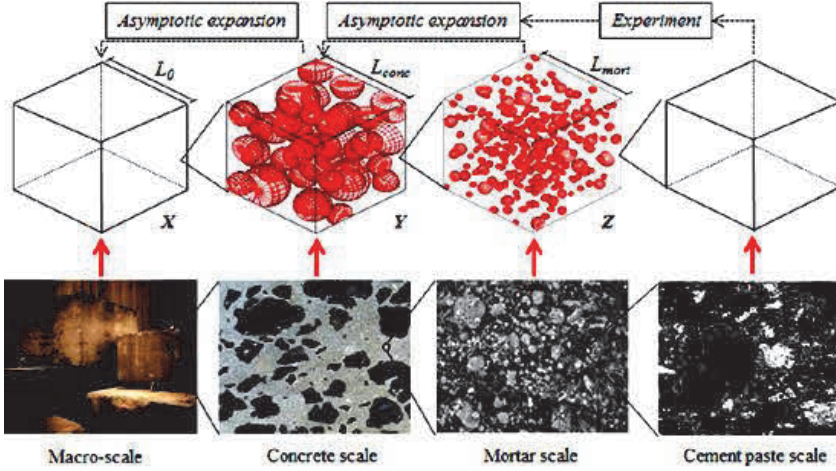


Figure 1: Scale division of concrete.

distributed randomly, as shown in Fig. 1. A spherical inclusion is defined by four parameters: the position of the center, depending on the parameters  $(y_1^n, y_2^n, y_3^n)$ , and the diameter  $D_{sand}$ . With regard to the specific RVE for mortar, its length,  $L_{mort}$ , is  $1cm$ , and the diameter of the spheres,  $D_{sand}$ , is  $0.25 - 1.0mm$ . It is worth of mention that  $(y_1^n, y_2^n, y_3^n)$  and  $D_{sand}$  are uniformly distributed within their own range. Thus, the RVE is further described with stochastic parameters, which can simulate the random distribution of sand in the cement paste.

At the concrete scale, the RVE is composed of the homogenized mortar as the matrix and coarse aggregates as the inclusion. A series of specific RVEs which can simulate the random distribution of coarse aggregates in the mortar, needs to be described in the same way as for the mortar scale, as shown in Fig. 1. The size of the RVEs of the concrete scale,  $L_{conc}$ , is  $20cm$ , and the diameter of the spheres is  $5 - 20mm$ .

Because of  $D_{sand} \ll L_{mort} \leq D_{aggr} \ll L_{conc} \ll L_0$ , where  $L_0$  characterizes the macro-scale, the requirement of separation of scales is satisfied.

### 3 A stochastic multi-scale model for autogenous shrinkage of concrete

#### 3.1 Governing equations

A point of a homogenous body can be treated as a periodic multiple permutation of the RVE which is heterogeneous in the asymptotic expansion theory, as shown in Fig. 2. When the equivalent homogenous body is subjected to external forces,

its field quantities such as the displacements, the stresses, and the strains, will vary with the global coordinate  $\mathbf{x}$ . Because of the great heterogeneity of the local constitution, they will also vary rapidly with the local coordinates  $\mathbf{y}$  and  $\mathbf{z}$ . Therefore, following the multi-scale representation of concrete, the scale factor  $\varepsilon_{conc}$  at the concrete scale is defined as  $\varepsilon_{conc} = \varepsilon$ , where  $\varepsilon$  denotes the basic scale factor. At the mortar scale, the scale factor  $\varepsilon_{mort}$  is defined as  $\varepsilon_{mort} = \varepsilon^2$ . For the sake of simplicity, the probability distributions  $w^{conc}$  and  $w^{mort}$  are collectively denoted as  $w$ , given as  $aw = \{w^{conc} : \mathbf{y} \in Y; w^{mort} : \mathbf{z} \in Z\}$ .

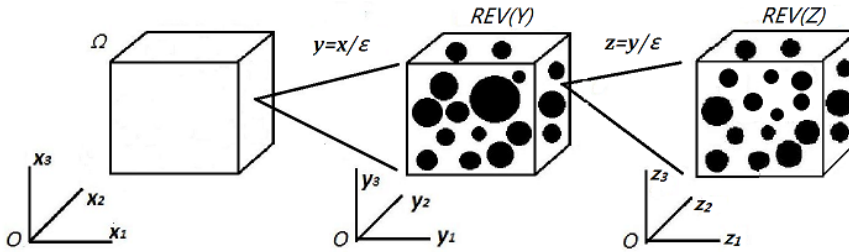


Figure 2: Representation of multi-scale method.

The governing differential equations for determination of the displacements of an elastic solid  $\Omega$  subjected to body forces are given as follows :

$$\frac{\partial}{\partial x_j} \left[ C_{ijkl}^\varepsilon(\mathbf{x}) \left( \frac{1}{2} \left( \frac{\partial u_k^\varepsilon(\mathbf{x})}{\partial x_l} + \frac{\partial u_l^\varepsilon(\mathbf{x})}{\partial x_k} \right) \right) \right] = f_i(\mathbf{x}), \quad \mathbf{x} \in \Omega \quad (1)$$

where, the body  $\Omega$  represents the elastic solid, consisting of the homogenized material on the macro-scale.  $u_i^\varepsilon(\mathbf{x})$  is a component of the displacement vector at point  $\mathbf{x}$  and  $f_i(\mathbf{x})$  is a component of the vector of body forces at this point.  $C_{ijkl}^\varepsilon(\mathbf{x})$  is a component of the elasticity tensor of the homogenized material. The boundary conditions are specified as follows:

$$u_i^\varepsilon(\mathbf{x}) = \bar{u}_i(\mathbf{x}), \quad \mathbf{x} \in \Gamma_u \quad (2)$$

$$v_j C_{ijkl}^\varepsilon(\mathbf{x}) \frac{1}{2} \left( \frac{\partial u_k^\varepsilon(\mathbf{x})}{\partial x_l} + \frac{\partial u_l^\varepsilon(\mathbf{x})}{\partial x_k} \right) = \bar{p}_i(\mathbf{x})_p, \quad \mathbf{x} \in \Gamma_p \quad (3)$$

$\Gamma_u$  is the part of the boundary  $\partial\Omega$  of  $\Omega$ , on which displacements  $\bar{u}_i(\mathbf{x})$  are specified, and  $\Gamma_p$  is the part of the boundary  $\partial\Omega$ , on which surface tractions  $\bar{p}_i(\mathbf{x})$  are specified. Therefore,  $\partial\Omega = \Gamma_u + \Gamma_p$ ;  $v_j$  denotes the unit normal vector on  $\Gamma_p$ .

However, autogenous shrinkage is the term for the bulk deformation of a closed, isothermal, cement-based material system, which is not subjected to external forces.

Therefore, the body forces and the boundary tractions are equal to zero. Modifying Eq. 1 for autogenous shrinkage results as

$$\frac{\partial}{\partial x_j} \left[ C_{ijkl}^\varepsilon(\mathbf{x}) \left( \frac{1}{2} \left( \frac{\partial u_k^\varepsilon(\mathbf{x})}{\partial x_l} + \frac{\partial u_l^\varepsilon(\mathbf{x})}{\partial x_k} \right) - \varepsilon_{kl}^\varepsilon(\mathbf{x}) \right) \right] = 0, \quad \mathbf{x} \in \Omega \quad (4)$$

where,  $\varepsilon_{kl}^\varepsilon(\mathbf{x})$  denotes the strain due to autogenous shrinkage. The properties of the material composition in the RVE can be expressed as

$$C_{ijkl}^\varepsilon(\mathbf{x}) = C_{ijkl}(\mathbf{y}, w^1) = C_{ijkl}(\mathbf{y}, \mathbf{z}, w^2) \quad (5)$$

### 3.2 Multi-scale analysis

Let  $\mathbf{x}$ ,  $\mathbf{y}$ ,  $\mathbf{z}$  denote the coordinate systems of the macro scale, the concrete scale and the mortar scale, respectively. They are related to one another as follows:

$$\mathbf{y} = \mathbf{x}/\varepsilon; \quad \mathbf{z} = \mathbf{y}/\varepsilon \quad (6)$$

An asymptotic expansion of  $\mathbf{u}^\varepsilon(\mathbf{x})$  is performed with the help of the coordinates  $\mathbf{x}$ ,  $\mathbf{y}$  and  $\mathbf{z}$ :

$$\mathbf{u}^\varepsilon(\mathbf{x}) = \mathbf{u}^0(\mathbf{x}) + \varepsilon \mathbf{u}^1(\mathbf{x}, \mathbf{y}, \mathbf{z}) + \varepsilon^2 \mathbf{u}^2(\mathbf{x}, \mathbf{y}, \mathbf{z}) + \dots \quad (7)$$

Differentiation with respect to  $\mathbf{x}$  is defined as

$$\frac{\partial}{\partial x_i} = \frac{\partial}{\partial x_i} + \varepsilon^{-1} \frac{\partial}{\partial y_i} + \varepsilon^{-2} \frac{\partial}{\partial z_i} \quad (8)$$

Substituting Eq.7 and Eq.8 into Eq.4 and letting  $\varepsilon \rightarrow 0$ , the coefficient of each term  $\varepsilon^n (n = -4, -3, -2, -1)$  must be zero.

The following partial differential equation is the vanishing coefficient of  $\varepsilon^{-4}$ :

$$\frac{\partial}{\partial z_j} \left( C_{ijkl}(\mathbf{y}, \mathbf{z}, w) \frac{\partial u_k^0}{\partial z_l} \right) = 0 \quad (9)$$

Since  $\mathbf{u}^0$  is only a function of  $\mathbf{x}$ , the above relation is automatically satisfied.

The following partial differential equation represents the vanishing coefficient of  $\varepsilon^{-3}$ :

$$\frac{\partial}{\partial y_j} \left( C_{ijkl}(\mathbf{y}, \mathbf{z}, w) \frac{\partial u_k^0}{\partial z_l} \right) + \frac{\partial}{\partial z_j} \left( C_{ijkl}(\mathbf{y}, \mathbf{z}, w) \left( \frac{\partial u_k^0}{\partial y_l} + \frac{\partial u_l^1}{\partial z_k} \right) \right) = 0 \quad (10)$$

Because  $\mathbf{u}^0$  is only a function of  $\mathbf{x}$ , the terms  $\partial u_k^0 / \partial z_l$  and  $\partial u_k^0 / \partial y_l$  vanish. Thus,  $\mathbf{u}^1$  is only a function of  $\mathbf{x}$  and  $\mathbf{y}$ , which can be written as follows:

$$u_i^1(\mathbf{x}, \mathbf{y}) = N_i^{kl}(\mathbf{y}) \frac{\partial u_k^0}{\partial x_l} \quad (11)$$

where,  $N_i^{kl}(\mathbf{y})$  is a coefficient of matrix function defined in the RVE(Y) at the concrete scale, which reflects the influence of the local heterogeneity of composites.

Recalling that  $u^0$  is only a function of  $\mathbf{x}$ , and  $u^1$  is a only function of  $\mathbf{x}$  and  $\mathbf{y}$ , the partial differential equation representing the vanishing coefficient of  $\varepsilon^{-2}$  can be simplified as follows:

$$\frac{\partial}{\partial z_j} \left[ C_{ijkl}(\mathbf{y}, \mathbf{z}, w) \left( \frac{\partial u_k^0}{\partial x_l} + \frac{\partial u_k^1}{\partial y_l} + \frac{\partial u_k^2}{\partial z_l} \right) \right] = 0 \quad (12)$$

The term  $\partial u_k^0 / \partial x_l$  is a function of  $\mathbf{x}$  and the term  $\partial u_k^1 / \partial y_l$  is a function of  $\mathbf{x}$  and  $\mathbf{y}$ . This allows writing  $u^2$  as follows:

$$u_i^2(\mathbf{x}, \mathbf{y}, \mathbf{z}) = M_i^{kl}(\mathbf{z}) \left( \delta_{km} \delta_{ln} + \frac{\partial N_k^{mn}}{\partial y_l} \right) \frac{\partial u_m^0}{\partial x_n} \quad (13)$$

where  $M_i^{kl}(\mathbf{z})$  is a coefficient of matrix function defined in the RVE(Z) at the mortar scale. It reflects the influence of the local configuration of the composites. Substituting Eq.11 and Eq.13 into Eq.12, gives:

$$\begin{aligned} & C_{ijkl}(\mathbf{y}, \mathbf{z}, w) \left( \frac{\partial u_k^0}{\partial x_l} + \frac{\partial u_k^1}{\partial y_l} + \frac{\partial u_k^2}{\partial z_l} \right) \\ &= C_{ijkl}(\mathbf{y}, \mathbf{z}, w) \left( \delta_{ks} \delta_{lt} + \frac{\partial M_k^{st}}{\partial z_l} \right) \left( \delta_{ms} \delta_{nt} + \frac{\partial N_s^{mn}}{\partial y_t} \right) \frac{\partial u_m^0}{\partial x_n} \end{aligned} \quad (14)$$

Substituting Eq.14 into Eq.12 yields the mortar scale equation for the domain Z, which is the equation for determination of  $M_i^{kl}(\mathbf{z})$ :

$$\frac{\partial}{\partial z_j} \left[ C_{ijkl}(\mathbf{y}, \mathbf{z}, w) \left( \delta_{ks} \delta_{lt} + \frac{\partial M_k^{st}}{\partial z_l} \right) \right] = 0 \quad (15)$$

It is seen that  $M_i^{kl}(\mathbf{z})$  only depend on  $\mathbf{z}$ .

The following simplified partial differential equation represents the vanishing coefficient of  $\varepsilon^{-1}$ :

$$\begin{aligned} & \frac{\partial}{\partial y_j} \left[ C_{ijkl}(\mathbf{y}, \mathbf{z}, w) \left( \frac{\partial u_k^0}{\partial x_l} + \frac{\partial u_k^1}{\partial y_l} + \frac{\partial u_k^2}{\partial z_l} \right) \right] \\ &+ \frac{\partial}{\partial z_j} \left[ C_{ijkl}(\mathbf{y}, \mathbf{z}, w) \left( \frac{\partial u_k^1}{\partial x_l} + \frac{\partial u_k^2}{\partial y_l} + \frac{\partial u_k^3}{\partial z_l} \right) \right] = 0 \end{aligned} \quad (16)$$

The volume average of quantities for the mortar scale domain Z is defined as

$$\langle \bullet \rangle_2 = \frac{1}{|Z|} \int_Z \bullet dz \quad (17)$$

Substitution of Eq.14 into Eq.16 and use of Eq.17 yields the following equation for determination of  $N_i^{kl}(\mathbf{y})$  in the RVE ( $\mathbf{Y}$ ) at the concrete scale:

$$\frac{\partial}{\partial y_j} \left[ C_{ijst}^{H_1}(\mathbf{y}, w) \left( \delta_{ms} \delta_{nt} + \frac{\partial N_s^{mn}}{\partial y_t} \right) \right] = 0 \quad (18)$$

where  $C_{ijst}^{H_1}(\mathbf{y}, w)$  is a component of the elasticity tensor of the homogenized mortar, which is given as

$$C_{ijst}^{H_1}(\mathbf{y}, w) = \frac{1}{|\mathbf{Z}|} \int_{\mathbf{Z}} C_{ijkl}(\mathbf{y}, \mathbf{z}, w) \left( \delta_{ks} \delta_{lt} + \frac{\partial M_k^{st}}{\partial z_l} \right) dz \quad (19)$$

Thus,  $N_i^{kl}(\mathbf{y})$  can be obtained from Eq.18, making use of Eq.19.

The following partial differential equation represents the vanishing coefficient of  $\epsilon^0$ :

$$\begin{aligned} & \frac{\partial}{\partial x_j} \left[ C_{ijkl}(y, z, w) \left( \frac{\partial u_k^0}{\partial x_l} + \frac{\partial u_k^1}{\partial y_l} + \frac{\partial u_k^2}{\partial z_l} \right) \right] + \frac{\partial}{\partial y_j} \left[ C_{ijkl}(y, z, w) \left( \frac{\partial u_k^1}{\partial x_l} + \frac{\partial u_k^2}{\partial y_l} + \frac{\partial u_k^3}{\partial z_l} \right) \right] \\ & + \frac{\partial}{\partial z_j} \left( C_{ijkl}(y, z, w) \left( \frac{\partial u_k^2}{\partial x_l} + \frac{\partial u_k^3}{\partial y_l} + \frac{\partial u_k^4}{\partial z_l} \right) \right) - \frac{\partial}{\partial x_j} (C_{ijkl}(y, z, w) \epsilon_{kl}^0(x)) = 0 \end{aligned} \quad (20)$$

The volume average of quantities for the mortar scale domain  $\mathbf{Y}$  is defined as

$$\langle \bullet \rangle_1 = \frac{1}{|\mathbf{Y}|} \int_{\mathbf{Y}} \bullet dy \quad (21)$$

Substitution of Eq.14 into Eq.20 with the help of Eq.17 and Eq.21 yields the following control equation for the concrete scale:

$$\frac{\partial}{\partial x_j} \left[ C_{ijkl}^H(w) \left( \frac{\partial u_k^0}{\partial x_l} - \epsilon_{kl}^0 \right) \right] = 0 \quad (22)$$

where,  $C_{ijkl}^H(w)$  is a component of the elasticity tensor of the homogenized the concrete scale, denoted as

$$C_{ijkl}^H(w) = \frac{1}{|\mathbf{Y}|} \int_{\mathbf{Y}} C_{ijst}^{H_1}(\mathbf{y}, w) \left( \delta_{ks} \delta_{lt} + \frac{\partial N_s^{kl}}{\partial y_t} \right) dy \quad (23)$$

Letting  $\epsilon \rightarrow 0$ , the strain field in the mortar scale domain  $\mathbf{Z}$  can be expressed as

$$\epsilon_{kl}^2 = \frac{1}{2} \left( \frac{\partial u_k^0}{\partial x_l} + \frac{\partial u_l^0}{\partial x_k} + \frac{\partial u_k^1}{\partial y_l} + \frac{\partial u_l^1}{\partial y_k} + \frac{\partial u_k^2}{\partial z_l} + \frac{\partial u_l^2}{\partial z_k} \right) \quad (24)$$

Having obtained  $\mathbf{N}(\mathbf{y})$  and  $\mathbf{M}(\mathbf{z})$  by solving Eq.15, Eq.18, and Eq.19;  $\mathbf{u}^1$  and  $\mathbf{u}^2$  can be obtained according to Eq.11 and Eq.13 respectively. Substituting  $\mathbf{u}^1$  and  $\mathbf{u}^2$  into Eq.24 gives

$$\begin{aligned} \varepsilon_{kl}^2 = & \frac{1}{2} \left( \frac{\partial u_k^0}{\partial x_l} + \frac{\partial u_l^0}{\partial x_k} \right) \\ & + \frac{1}{2} \frac{\partial u_m^0}{\partial x_n} \left[ \left( \delta_{pm} \delta_{qn} + \frac{\partial N_p^{mn}}{\partial y_q} \right) \left( \frac{\partial M_k^{pq}}{\partial z_l} + \frac{\partial M_l^{pq}}{\partial z_k} \right) + \left( \frac{\partial N_k^{mn}}{\partial y_l} + \frac{\partial N_l^{mn}}{\partial y_k} \right) \right] \end{aligned} \quad (25)$$

where the strains of the matrix in the domain  $\mathbf{Z}$  are the strains of the cement paste  $\varepsilon_{c-p}$ . They can be obtained from tests, which can be operated easily, and they provide results of high precision. Thus, the homogenized displacement field  $\mathbf{u}^0$  can be computed, followed by determination of  $\mathbf{u}^1$  and  $\mathbf{u}^2$ . The strain field in the concrete scale domain  $\mathbf{Y}$  is then defined as follows:

$$\varepsilon_{kl}^1 = \frac{1}{2} \left( \frac{\partial u_k^0}{\partial x_l} + \frac{\partial u_l^0}{\partial x_k} + \frac{\partial u_k^1}{\partial y_l} + \frac{\partial u_l^1}{\partial y_k} \right) \quad (26)$$

Substitution of Eq.11 into Eq.26 gives

$$\varepsilon_{kl}^1 = \frac{1}{2} \left( \frac{\partial u_k^0}{\partial x_l} + \frac{\partial u_l^0}{\partial x_k} \right) + \frac{1}{2} \frac{\partial u_m^0}{\partial x_n} \left( \frac{\partial N_k^{mn}}{\partial y_l} + \frac{\partial N_l^{mn}}{\partial y_k} \right) \quad (27)$$

where, the strains of the matrix in the domain  $\mathbf{Y}$  are the strains of the homogenized mortar,  $\varepsilon_{mort}$ . Substitution of  $\mathbf{u}^0$  into Eq.22 and use of Eq.23, the homogenized strains  $\varepsilon^0$  of the macro-scale, caused by autogenous shrinkage, are obtained.

## 4 Analysis procedure

### 4.1 Computation of homogenized autogenous shrinkage

According to the RVE the mortar and the concrete scale, different inclusions, such as sand and coarse aggregates, have different size and positions in different samples. From the multi-scale Eq.19 and Eq.23, it can be seen that this configuration has an influence on the stiffness of concrete, which also means on autogenous shrinkage. Thus, as was mentioned in the context of the description of mortar and concrete scale, the characteristics of the homogenized concrete, can be evaluated by means of the proposed multi-scale model.

- Based on the statistical characteristics of mortar scale, for a random distribution  $w_{s,mort}$ , a sample is generated. Then, Eq.15 is solved in RVE ( $\mathbf{Z}$ ) to obtain  $\mathbf{M}(\mathbf{z}, w_{s,mort})$ . Thereafter, the homogenized elastic tensor  $\mathbf{C}^{H1}(\mathbf{y}, w_{s,mort})$ , corresponding to sample  $w_{s,mort}$ , is computed by means of Eq.19.

- Analogous to ahead, for a random distribution  $w_{s,conc}$  at the concrete scale, a sample is generated. Then, Eq.18 is solved in RVE ( $Y$ ) to obtain  $\mathbf{N}(\mathbf{y}, w_{s,conc})$ . Thereafter, the homogenized elastic tensor  $\mathbf{C}^H(\mathbf{x}, w_{s,mort}, w_{s,conc})$ , corresponding to sample  $w_{s,conc}$ , is computed by means of Eq.23.
- Substitute  $\mathbf{N}(\mathbf{y}, w_{s,conc})$  and  $\mathbf{M}(\mathbf{z}, w_{s,mort})$  into Eq.11 and Eq.13, the strain field  $\boldsymbol{\varepsilon}^2(\mathbf{z}, w_{s,mort})$  in the domain  $Z$  at the mortar scale as a function of  $\mathbf{u}^0(\mathbf{x}, w_{s,mort}, w_{s,conc})$  is determined with the help of Eq.25. The strains of the matrix are the strains of cement paste  $\boldsymbol{\varepsilon}_{c-p}$ ; thus,  $\mathbf{u}^0(\mathbf{x}, w_{s,mort}, w_{s,conc})$  is computed, followed by  $\mathbf{u}^1(\mathbf{y}, w_{s,conc})$  and  $\mathbf{u}^2(\mathbf{z}, w_{s,mort})$ .
- Compute the homogenized strains  $\boldsymbol{\varepsilon}^0(\mathbf{x}, w_{s,mort}, w_{s,conc})$  of the concrete, caused by autogenous shrinkage, by substituting  $\mathbf{u}^0(\mathbf{x}, w_{s,mort}, w_{s,conc})$  into Eq. 22-24.
- Following the generation of  $T$  samples with random distributions  $w_s = \{w_{s,conc} : \mathbf{y} \in Y; w_{s,mort} : \mathbf{z} \in Z\}$ ,  $s = 1, 2, \dots, T$ , and Based on the Kolmogorov's strong law of large numbers, the strains representing the homogenized material can be computed by means of the equation:

$$\bar{\boldsymbol{\varepsilon}}(\mathbf{x}) = \frac{\sum_{s=1}^T \boldsymbol{\varepsilon}^0(\mathbf{x}, w_{s,mort}, w_{s,conc})}{T}, \quad T \rightarrow \infty \quad (28)$$

## 4.2 Flowchart of multi-scale algorithm

The flowchart of the algorithm for the proposed stochastic multi-scale method for prediction of the autogenous shrinkage of concrete is given as follows:

## 5 Model validation

The main purpose of this Chapter is to validate the capability of the proposed multiscale technique to predict autogenous shrinkage of early-age concrete by means of upscaling from the cement paste scale. Thus, a set of tests for autogenous deformations of the cement paste, the mortar, and the concrete was conducted and used for validation at the mortar and the concrete scale.

### 5.1 Validation experiments on the cement paste, the mortar, and the concrete

#### 5.1.1 Materials and mix design

OPC (Ordinary Portland Cement) was used as a cementitious material. The chemical composition and the physical properties of cementitious materials are given

Table 1: Flowchart for computing the autogenous shrinkage of concrete.

Input		$E_{c-p}, \nu_{c-p}; E_{sand}, \nu_{sand}$ ; diameter distribution of sand, $D_{sand}$ ; volume fraction of sand, $f_{sand}$ ; $E_{aggr}, \nu_{aggr}$ ; diameter distribution of coarse aggregate, $D_{aggr}$ ; volume fraction of the coarse aggregate, $f_{aggr}$ ; autogenous shrinkage of cement paste achieved from test $\epsilon_{c-p}$
Mortar scale	(1)	Generate a sample REV (Z) with a random distribution $w_{s,mort}$ , which consists of cement paste as the matrix and randomly distributed sphere which simulate the sand inclusions, as shown in Fig. 1; establish a finite element model for the REV (Z), consisting of tetrahedron elements with 10-nodes, as shown in Fig. 8
	(2)	Compute $\mathbf{M}(\mathbf{z})$ in REV (Z) by solving Eq.15, and evaluate the elasticity tensor $C_{ijst}^{H_1}(y, w)$ of the homogenized mortar from Eq.19
Concrete scale	(3)	Generate a sample REV (Y) with a random distribution $w_{s,conc}$ , which consists of the homogenized mortar as the matrix and randomly distributed sphere which simulate sand inclusion, as shown in Fig. 1; establish a finite element model for the REV (Y), consisting of tetrahedron elements with 10-nodes, as shown in Fig. 8
	(4)	Compute $\mathbf{N}(\mathbf{y})$ in REV Y by solving Eq.18, and evaluate the elasticity tensor $C_{ijst}^H(y, w)$ of the homogenized the concrete scale from Eq.23
	(5)	Compute $\mathbf{u}^0$ with the help of Eq.25, where the strains of the matrix are the strains of cement paste $\epsilon_{c-p}$
	(6)	Compute the strain field $\boldsymbol{\epsilon}^I$ in the domain Y at the concrete scale with the help of Eq.27 and Eq.28
Macro-scale	(7)	Compute the homogenized strains $\boldsymbol{\epsilon}^0$ of the concrete by substituting $\mathbf{u}^0$ into Eq. 22-24.
	(8)	Based on Kolmogorov's strong law of large numbers, the strains of the homogenized material can be computed Eq.28.
Output		$C_{ijst}^{H_1}(y, w), C_{ijst}^H(y, w), \boldsymbol{\epsilon}_{mort}, \bar{\boldsymbol{\epsilon}}(\mathbf{x})$

in Tab. 2. Graded and crushed limestone, 5-20mm, with a maximum of 20mm, conforming to ASTM C33 (Standard Specification for Concrete Aggregates), were used as coarse aggregates, whereas graded river sand, 0.25-1.0mm with a maximum size of 1.0mm, conforming to ASTM C33, was used as a fine aggregate. The physical properties of the aggregates are given in Tab. 3. A commercially available high-range water reducing admixture (HRWRA), conforming to ASTM C494 Type F (Specification for Chemical Admixtures for Concrete), was used in this study.

Table 2: Chemical composition and physical properties of cement.

Item	Blaine ( $\text{cm}^2/\text{g}$ )	Specific gravity ( $\text{g}/\text{cm}^3$ )	Chemical composition (%)					
			SiO <sub>2</sub>	Al <sub>2</sub> O <sub>3</sub>	Fe <sub>2</sub> O <sub>3</sub>	CaO	MgO	SO <sub>3</sub>
OPC	3413	3.15	21.01	6.40	3.12	61.33	3.02	2.14

Table 3: Physical properties of aggregates.

Item	Specific gravity ( $\text{g}/\text{cm}^3$ )	Fineness modulus	Water absorption (%)	Volumetric weight ( $\text{kg}/\text{m}^3$ )
River sand	2.67	2.60	1.83	1422
Coarse aggregate	2.63	6.87	0.63	1429

The mixture proportioning of the cement paste, the mortar, and the concrete are shown in Tab. 4, Tab. 5, and Tab. 6, respectively. Except for the graded river sand that has been added, the mortar has the same composition as the corresponding net cement paste, including the amount of HRWRA. Also, the concrete has the same composition as the corresponding mortar except for the addition of graded and crushed limestone as coarse aggregates. It is worth of mention that a contrasting test with different volume fractions of coarse aggregates was included in the concrete series. The percentage in brackets refers to the volume fraction.

Table 4: Mix design of the cement paste (g).

Serial number	w/c	Cement	Water	HRWRA
P1	0.3	400	120	4

Table 5: Mix design of the mortar (g).

Serial number	w/c	Cement	Water	Sand	HRWRA
M1	0.3	400	120	900 (40%)	4

### 5.1.2 Specimen preparation and test method

For the cement paste and the mortar, a test method conforming to ASTM C1698-09 (Standard Test Method for Autogenous Strain of Cement Paste and Mortar) was

Table 6: Mix design of the concrete (kg/m<sup>3</sup>).

Serial number	w/c	Cement	Water	Sand	Coarse agg.	HRWEA
C1	0.3	390	117	876 (40%)	1018 (40%)	5
C2	0.3	390	117	876 (40%)	822 (35%)	5
C3	0.3	390	117	876 (40%)	655 (30%)	5

chosen. The cement paste (P1) and the mortar (M1) were freshly mixed according to ASTM C305 (Practice for Mechanical Mixing of Hydraulic Cement Pastes and Mortars of Plastic Consistency). Three specimens of each mixture proportion were prepared, using a corrugated mold which is sealed to prevent moisture loss. It offers little resistance to a length change of the specimen, as shown in Fig. 3. The length of the specimen was measured, using a dial gauge at regular time intervals until the designed age. The change in length and the original length of the specimen were used to compute the autogenous strain.

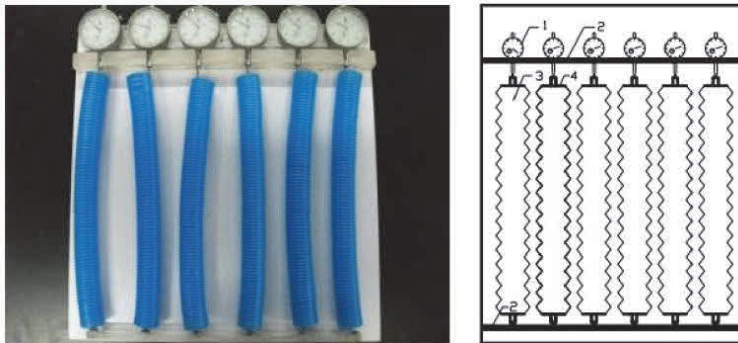


Figure 3: Corrugated mold and measure device for the cement paste and the mortar.

For the concrete, the ingredients were mixed in the laboratory, conforming to ASTM C192/192M (Standard Practice for Making and Curing Concrete Test Specimens in the Laboratory). A few steel probes were embedded in the concrete, penetrating the hole at the ends of the steel mold of 100 mm × 100 mm × 515 mm. A teflon sheet of 1 mm thickness was placed on the bottom of the mold for free movement of the specimen. Then, for each mixture proportion, three identical prismatic specimens were cast in the specific steel mold and subjected to full vibration on the vibration table. At last, all specimens were covered with a polyester film of 0.1mm thickness to avoid evaporation and absorption of outside moisture, as shown in Fig. 4. After removal of the steel mold, 12 hours after mixing, all specimens were stored

at a control condition set by a temperature of  $20\pm 2^{\circ}\text{C}$  and a relative humidity of  $90\pm 5\%$ . The dial gauge and a support were used as a measuring instrument, as shown in Fig. 4.



(a) Specimens of the concrete

(b) Measure device of the concrete

Figure 4: Specimens and measure device of the concrete.

The test method for the cement paste and the mortar, conforming to ASTM C1698-09, can measure the autogenous deformations from the time of final setting. For the concrete, however, the first measurement was only carried out after removal of the mold, 12 hours after mixing, when the steel probes embedded in the concrete were sufficiently stable and the molds were easy to be removed without damage to the specimens. Thus, considering the purpose of these contrasting tests at different scales, the measurement at 12 hours after mixing was taken as the relative zero point.

The average of the experimental values, obtained from two identical specimens of the size  $25\text{ mm}\times 25\text{ mm}\times 100\text{ mm}$ , was taken to determine the elastic modulus of the cement paste and the mortar in accordance with ASTM C469 (Standard Test Method for Static Modulus of Elasticity and Poisson Ratio of Concrete in Compression).

### 5.1.3 Results and discussion

From the values of length change, the free shrinkage strains are computed at 1, 3, 5, 7, 14 and 28 days, in terms of microstrain for each individual mix.

Fig. 5 shows the autogenous shrinkage of the cement paste, the mortar, and concrete C1 as a function of time. It is obvious that autogenous shrinkage of the cement paste, the mortar, and the concrete decreases in consequence of the addition of sand and coarse aggregates, which restrain the deformation of the cement paste. At 28 days, autogenous shrinkage of the cement paste, the mortar, and of concrete C1

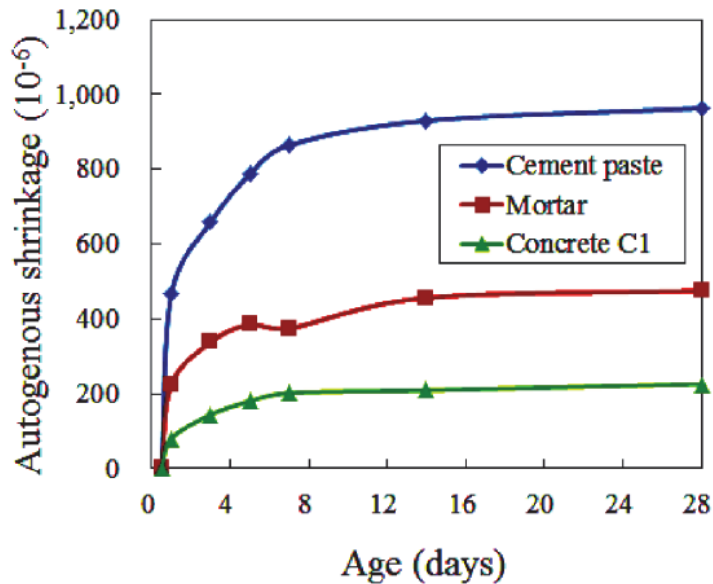


Figure 5: Autogenous shrinkage of the cement paste, the mortar and the concrete C1.

were  $963 \times 10^{-6}$ ,  $475 \times 10^{-6}$  and  $226 \times 10^{-6}$ , respectively. However, the evolution of autogenous shrinkage of these three materials is similar. During the first day, there was a rapid increase of autogenous shrinkage, then its rate was decreasing between one day and seven days, and at about 14 days, it became almost zero. Thus, it can be concluded that autogenous shrinkage occurs mainly during the first seven days, after which it has reached 89.7%, 83.2%, and 89.4%, respectively, of the total autogenous shrinkage. This fact can be explained by the mechanism of autogenous shrinkage, which is associated with the reduction of the internal volume of the cement/water mixture caused by the hydration process [Zhang, Hou and Wei (2010)]. It is well known that the stress state in the liquid phase follows the law of surface tension: the smaller the pore size, the larger the pressure difference at the interface between the liquid and the gaseous phase [Pichler, Lackner and Mang (2007)]. Therefore, as the degree of liquid saturation decreases, the location of this interface moves into smaller pores, resulting in an increase of capillary depression in the liquid phase. This causes a contraction of the solid phase, which is macroscopically observable as autogenous shrinkage [Lura and Jensen (2003)]. Along with the growth of age, the hydration rate decreases, resulting in a slower increase of autogenous shrinkage.

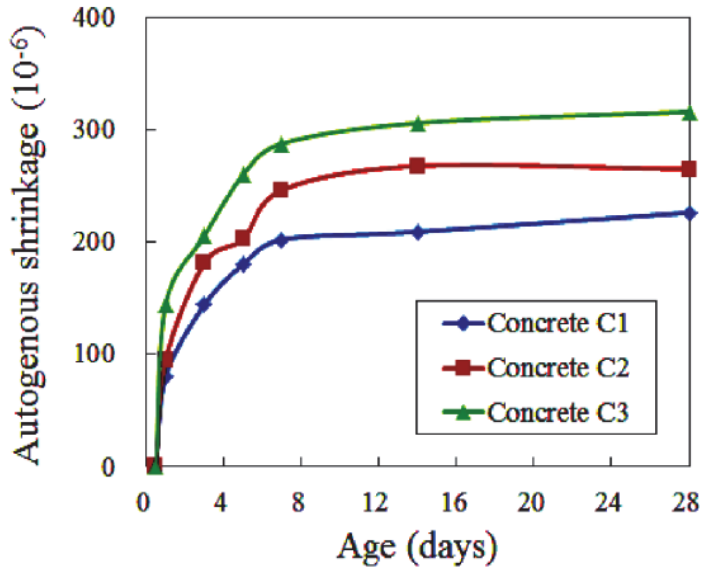


Figure 6: Autogenous shrinkage of the concrete C1, C2 and C3.

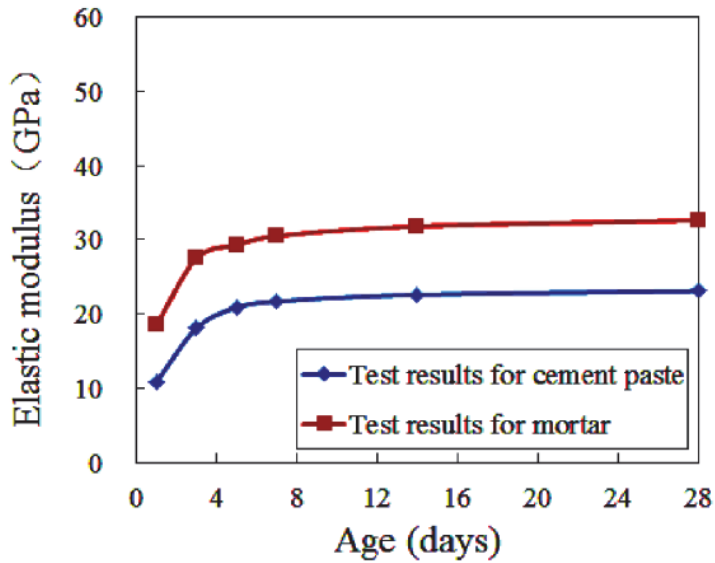


Figure 7: Elastic modulus of the cement paste and the mortar.

Fig. 6 refers to autogenous shrinkage of the concrete C1, C2, and C3, characterized by different volume fractions of coarse aggregates. It is seen that autogenous shrinkage decreases with increasing volume fraction of the aggregate. At 28 days, autogenous shrinkage of concrete C1 (40%), C2 (35%), and C3 (30%) was  $226 \times 10^{-6}$ ,  $265 \times 10^{-6}$  and  $316 \times 10^{-6}$ , respectively. The trend of the development of autogenous shrinkage is the same for C1, C2, and C3. The main reason for this is the internal restraint between the randomly distributed aggregates and the mortar matrix, resulting in restrained deformations of the matrix. Thus, the larger the volume fraction of the coarse aggregate, the smaller the shrinkage of the corresponding concrete.

Fig. 7 shows the elastic modulus of the cement paste and of the mortar as a function of age. During the first three days, the elastic modulus of both the cement paste and the mortar increases significantly. It may reach about 85% of the values at 28 days. As regards Fig. 7, the value of the elastic modulus at 3 days and 28 days, respectively, are 19.1 GPa and 23.1 GPa for the cement paste, and 30.5 GPa and 33.8 GPa for the mortar. The reason for the higher values of the elastic modulus for the mortar than for the cement paste is the addition of sand.

## ***5.2 Comparison of model predictions with experimental results***

As mentioned above, the evaluation of autogenous shrinkage of early-age concrete was based on the following main assumptions: (a) concrete was considered as a three-scale composite medium, composed of cement paste and sand at the mortar scale, of homogenized mortar and coarse aggregate at the concrete scale, and of a homogenized isotropic continuum at the macro-scale; (b) the heterogenous mortar scale and the concrete scale were modeled by periodic RVEs.

The multi-scale formulation described in Chapter 3 was implemented with the help of the finite element method. Typical finite element meshes employed in the present study are shown in Fig. 8. The length of the RVE at the mortar scale is 1cm, while the length of the RVE at the concrete scale is 20cm.

The predictive capacity of the model was determined by calculating autogenous shrinkage and comparing the results with experimentally obtained corresponding values at the mortar and the concrete scale, as shown in Fig. 9 and Fig. 10. It is seen that the numerical the results from the proposed model are slightly smaller than results from the experiment. On the one hand, this is a consequence of a series of simplifying assumptions, one of which is that the mortar and the concrete are regarded as inclusions dispersed in the homogenous matrix, with perfect bond between them. Moreover, the influence of micro-cracking on the stiffness is disregarded. On the other hand, the movement of the specimens during the test and drying shrinkage caused by a non-ideal test environment may result in a measure-

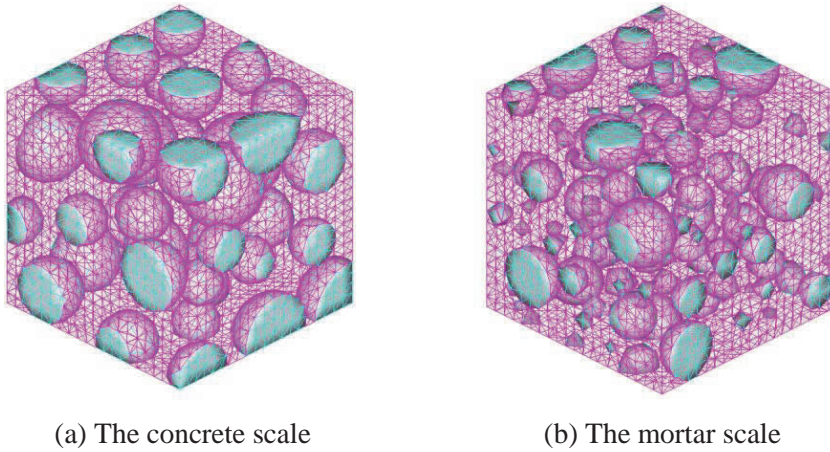


Figure 8: The finite element discretization of REV by means of tetrahedral.

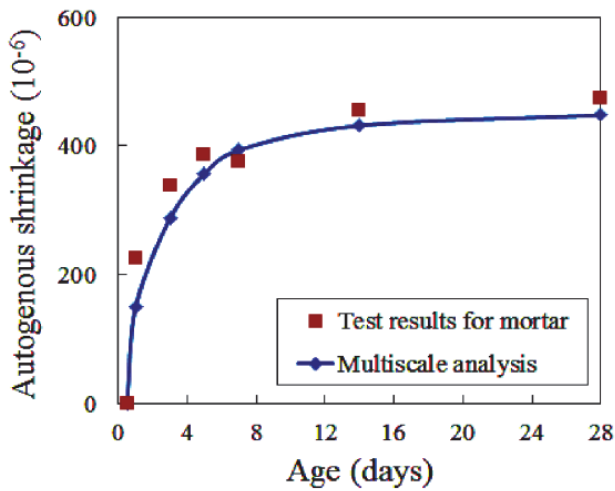


Figure 9: Comparison between test and multiscale model for the mortar.

ment error. Thus, taking all of these factors into consideration, it is fair to say that good agreement between the numerical predictions and the experimental data was obtained in this study, with a correlation coefficient of up to  $R^2 = 94.59\%$ . Thus, it may be concluded that the proposed model is quite effective.

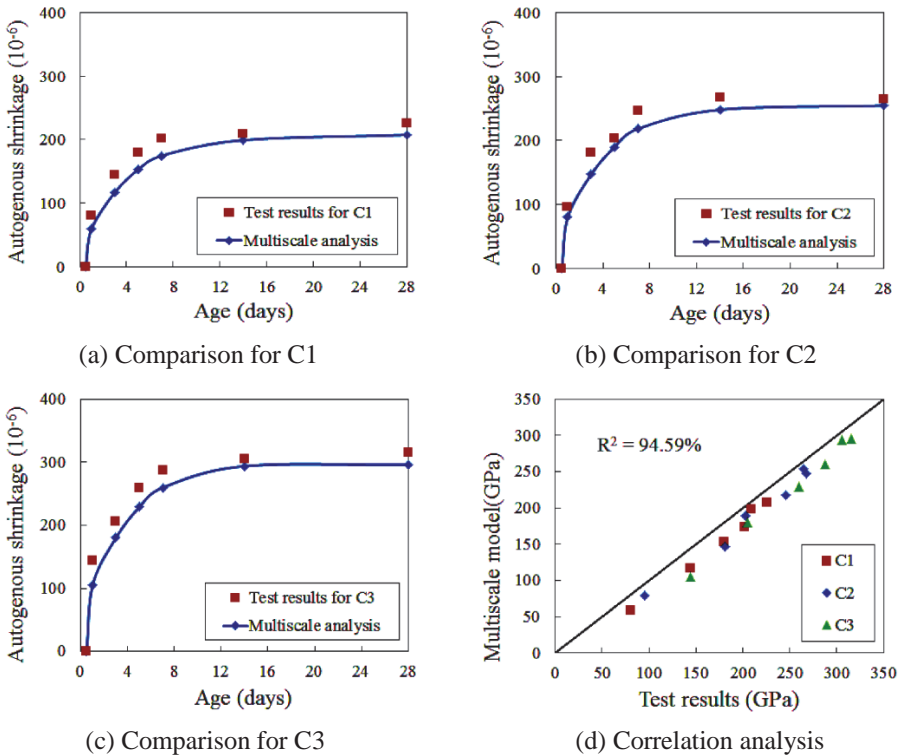


Figure 10: Comparison between test and multiscale model for the concrete C1, C2 and C3.

## 6 Discussion

This Chapter, contains a report on the influence of the type of the aggregate, including coarse and fine aggregates. This influence was investigated by a cross-scale study on upscaling of autogenous shrinkage from the cement paste scale. For coarse aggregates, for the purpose of a comparison, crushed and graded siliceous aggregate (quartzite), igneous aggregate (granite), and calcareous aggregate (limestone) were chosen, whereas for fine aggregates, river sand, manufactured lime sand, and manufactured granite sand were selected. The modulus of elasticity and Poisson's ratio are given in Tab. 7 [Chang and Zhang (2007)].

Fig. 11 shows a comparison of autogenous shrinkage of concrete with river sand as fine aggregate and different kinds of coarse aggregates. Firstly, the development of autogenous shrinkage is similar for these three coarse aggregates, and secondly, autogenous shrinkage of concrete with calcareous aggregates (limestone) is obvi-

Table 7: Mechanical properties of coarse aggregate.

Type	E (GPa)	Poisson's ratio
Quartzite	27.9-69.3	0.17-0.36
Granite	24.8-61.1	0.12-0.27
limestone	29.4-84.2	0.18-0.35

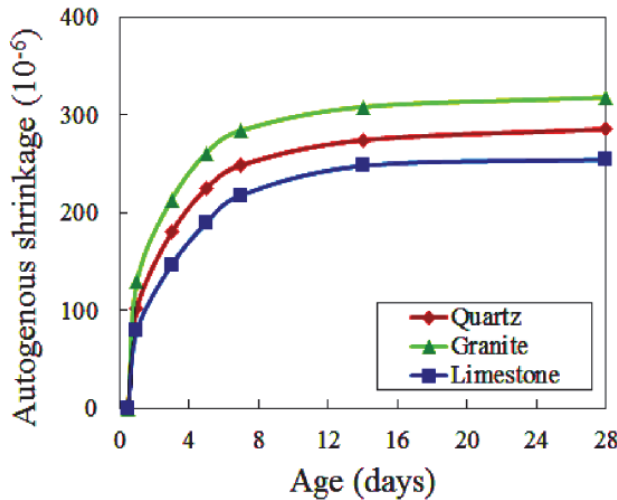


Figure 11: Autogenous shrinkage of concrete with different kinds of coarse aggregates.

ously smaller than that of concrete with igneous aggregates (granite). For concrete with siliceous aggregates (quartzite), autogenous shrinkage falls in between autogenous shrinkage of concrete with the other two aggregates. At 28 days, autogenous shrinkage of concrete with limestone aggregates, quartzite aggregates, and granite aggregates is  $250 \times 10^{-6}$ ,  $282 \times 10^{-6}$ , and  $320 \times 10^{-6}$ , respectively. After gradual stabilization at later ages, autogenous shrinkage of concrete with limestone decreases by 43.4% relative to the mortar matrix. The corresponding reductions for concrete with quartzite and granite are 36.2% and 27.6%, respectively. This phenomenon can be explained by the configuration and the properties of the constituents. The only variable in this comparison is the modulus of elasticity. The higher the elastic modulus of the coarse aggregates, the higher is the elastic modulus of concrete and the stronger is the restraint on the deformations of the matrix, which, macroscopically, results in smaller autogenous shrinkage of concrete.

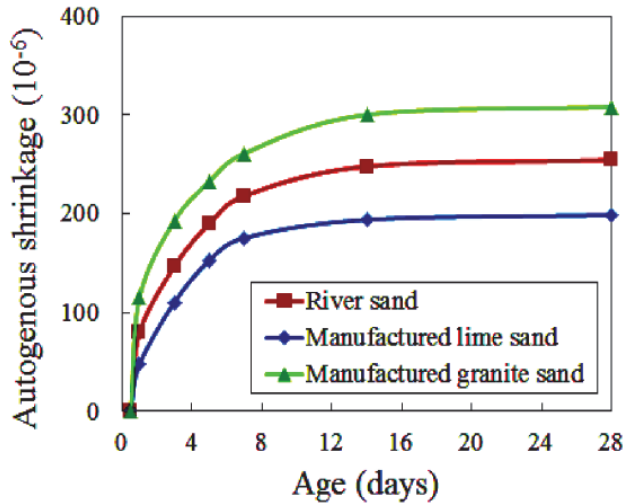


Figure 12: Autogenous shrinkage of concrete with different kinds of fine aggregates.

Fig. 12 shows a comparison of autogenous shrinkage of concrete for different kinds of fine aggregates and the same coarse aggregate (limestone). Firstly, it is seen that autogenous shrinkage of concrete with manufactured lime sand is smaller than that of concrete with manufactured granite sand, while for concrete with river sand it falls between the other two. This situation is similar to the one shown in Fig. 11. The reason for this is that the main composition of river sand is quartz and that manufactured lime and granite sand are obtained by means of crushing of limestone and granite, respectively. Thus, their mechanical properties are the same as the ones of the coarse aggregates. Secondly, the difference in autogenous shrinkage for different kinds of fine aggregates is greater than the one for different kinds of coarse aggregates, as follows from a comparison of Fig. 12 with Fig. 11. This can be explained by the grain sizes of the aggregates. The maximum size of river sand is 1mm, the one of manufactured lime and granite sand is 4.75mm, whereas the one of coarse aggregates is 20mm. That is to say, the specific surface area of fine aggregates is larger than that of coarse aggregates, which results in a stronger constraint of the matrix. Therefore, the difference between different aggregates is amplified.

Fig. 13 refers to the combined optimum of fine and coarse aggregates for autogenous shrinkage at 28 days. It is seen that the smallest value is obtained for manufactured lime sand with limestone coarse aggregates as  $199 \times 10^{-6}$ . Then comes

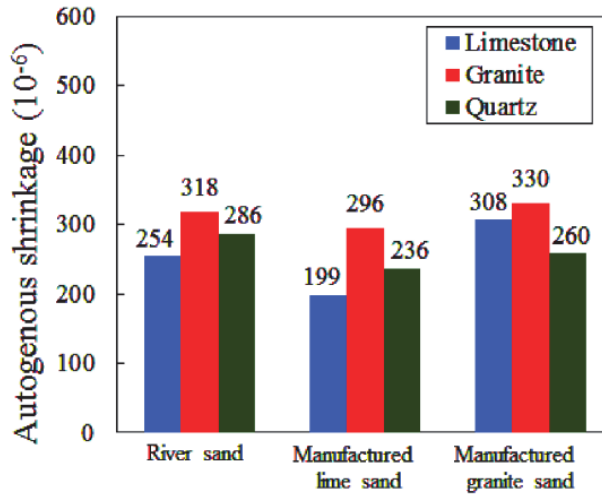


Figure 13: Combinatorial optimization of fine and coarse aggregate.

manufactured lime sand with quartz coarse aggregates as  $236 \times 10^{-6}$ . If these two combinations are not available, river sand with limestone coarse aggregates and manufactured granite sand with quartz coarse aggregates are reasonable substitutions. Thus, it can be concluded from the above discussion that the type of the aggregate has an important influence on autogenous shrinkage of concrete. Crushed and graded manufactured lime sand with limestone coarse aggregates appear to be the best choice for engineering practice in order to reduce autogenous shrinkage.

## 7 Summary and Conclusions

In this research, a stochastic multiscale model for cement-based materials, focusing on the prediction of autogenous shrinkage, was presented. This model accounts for the hydration process of cement and the random distribution of aggregates. In addition to the formulation of the underlying multiscale framework, including representation of the division of scales, a specific RVE was established and the appropriate upscaling schemes, based on asymptotic expansion theory, were presented. Experimental results were obtained from a set of tests considering autogenous deformations of the cement paste, the mortar, and the concrete. They were used to validate the predictive capability of the developed numerical model. Finally, macroscopic autogenous shrinkage, obtained from upscaling from the cement paste scale, was investigated; different kinds of aggregates were chosen to study the influence of these kinds and of the volume fractions. Finally, the combined optimum of fine and

coarse aggregates was determined. The following conclusions can be drawn:

- By means of comparing the model predictions with experimental results, the proposed model was validated successfully.
- Autogenous shrinkage occurs mainly during the first seven days, where about 80% of autogenous shrinkage at 28 days may be reached. Autogenous shrinkage is clearly tied to the hydration process.
- Autogenous shrinkage of the cement paste, the mortar, and the concrete decreases in case of adding sand and coarse aggregates. This results in a restraint of the deformation of the cement paste. The larger the volume fraction of coarse aggregates, the smaller the shrinkage of corresponding concrete will be.
- The type of the aggregate has a great influence on autogenous shrinkage of concrete. Crushed and graded manufactured lime sand with limestone coarse aggregate are found to be the best choice to reduce autogenous shrinkage.

In the proposed model, the mechanical properties and autogenous shrinkage of cement paste are obtained directly from experiments, which are standardized and highly precise from the beginning of the set. Thus, the described cross-scale research from the cement paste to the macro structure of concrete avoids non-standardized, highly specialized tests of concrete, including the embarrassing specification of the starting time. Moreover, performance-based optimization of cement-based materials becomes possible. Improvements of the model as regards treatment of cement hydration which will focus on the mixture characteristics and the cement chemistry are topics of ongoing research.

**Acknowledgement:** Financial support of this research by the National Basic Research Program of China (973 Program: 2011CB013800) and the National Natural Science Foundation of China (50908167 and 50838004), is gratefully acknowledged. In addition, special thanks are offered to Professor J.Z. Cui and Doctor X.F. Guan to the great help to complete this paper.

## References

**ACI Committee 209** (2009): *Prediction of creep, shrinkage, and temperature effects in concrete structures* (ACI 209R-92). Farmington Hills (MI): American Concrete Institute.

**Barcelo, L.; Boivin, S.** (1999): *Linear and volumetric autogenous shrinkage measurements: material behavior or experimental artifact*. In: Persson B, Fagerlund G, editors. Proceedings of the Second Int. Research Seminar: Self-desiccation and its Importance in Concrete Technology, Lund, Sweden, pp. 109–125.

**Bjøntegaard, O.; Hammer, T. A.; Sellevold, E. J.** (2004): On the measurement of free deformation of early age cement paste and concrete. *Cement and Concrete Composites*, vol. 26, no. 5, pp. 427–435.

**Böhm, H. J.; Han, W.; Eckschlager, A.** (2004): Multi-inclusion unit cell studies of reinforcement stresses and particle failure in discontinuously reinforced ductile matrix composites. *CMES: Computer Modeling in Engineering and Sciences*, vol. 5, no. 1, pp. 5-20.

**Chang, S. P.; Zhang, S. M.** (2007): *Engineering geology manual*, fourth edition, Building Industry Press, Beijing, China (in Chinese).

**Chu, I.; Kwon, S. H.; Amin, M. N.; Kim, J. K.** (2012): Estimation of temperature effects on autogenous shrinkage of concrete by a new prediction model. *Construction and Building Materials*, vol. 35, pp. 171–182.

**Constantinides, G.; Ulm, F. J.** (2004): The effect of two types of C–S–H on the elasticity of cement-based materials: results from nano-indentation and micromechanical modeling. *Cement and Concrete Research*, vol. 34, no. 1, pp. 67-80.

**Cui, J. Z.; Cao, L. Q.** (1998): Finite element method based on two-scale asymptotic analysis. *Mathematica. Numerica. Sinica*, vol. 20, no. 1, pp. 89-102.

**Darquennes, A.; Staquet, S.; Marie, P. D. O.; Bernard, E.** (2011): Effect of autogenous deformation on the cracking risk of slag cement concretes. *Cement and Concrete Composites*, vol. 33, no. 3, pp. 368–379.

**Dong, L. T.; Atluri, S. N.** (2013): Development of 3D Trefftz Voronoi Cells with Ellipsoidal Voids &/or Elastic/Rigid Inclusions for Micromechanical Modeling of Heterogeneous Materials. *CMC: Computers, Materials & Continua*, vol. 30, no. 1, pp. 39-81.

**Dong, L. T.; Atluri, S. N.** (2012): T-Trefftz Voronoi cell finite elements with elastic/rigid inclusions or voids for micromechanical analysis of composite and porous materials. *CMES: Computer Modeling in Engineering and Sciences*, vol. 83, no. 2, pp. 183-219.

**Dong, L. T.; Atluri, S. N.** (2013): SGBEM Voronoi Cells (SVCs), with embedded arbitrary-shaped inclusions, voids, and/or cracks, for micromechanical modeling of heterogeneous materials. *CMC: Computers, Materials & Continua*, vol. 33, no. 2, pp. 111-154.

**Dong, L. T.; Gamal, S. H.; Atluri, S. N.** (2013): Stochastic Macro Material Prop-

erties, Through Direct Stochastic Modeling of Heterogeneous Microstructures with Randomness of Constituent Properties and Topologies, by Using Trefftz Computational Grains (TCG). *CMC: Computers, Materials & Continua*, vol. 37, no. 1, pp. 1-21.

**Gaurav, S.** (2012): The influence of temperature on autogenous volume changes in cementitious materials containing shrinkage reducing admixtures. *Cement and Concrete Composites*, vol. 34, no. 7, pp. 855-865.

**Holt, E. E.; Leivo, M. T.** (2006): Cracking risk associated with early age shrinkage. *Cement and Concrete Composites*, vol. 26, no. 5, pp. 521–530.

**Idiart, A.; Bisschop, J.; Caballero, A.; Lura, P.** (2012): A numerical and experimental study of aggregate-induced shrinkage cracking in cementitious composites. *Cement and Concrete Research*, vol. 42, no. 2, pp. 272–281.

**Kar, A.; Ray, I.; Unnikrishnan, A.; Davalos, J. F.** (2013): Composite modeling to predict shrinkage of concretes containing supplementary cementitious materials from paste volumes. *Construction and Building Materials*, vol. 43, pp. 139–155.

**Kohno, K.; Okamoto, T.; Isikawa, Y.; Mori, H.** (1999): Effects of artificial lightweight aggregate on autogenous shrinkage of concrete. *Cement and Concrete Research*, vol. 29, no. 4, pp. 611–614.

**Lee, K. M.; Lee, H. K.; Lee, S. H.; Kim, G. Y.** (2006): Autogenous shrinkage of concrete containing granulated blast-furnace slag. *Cement and Concrete Research*, vol. 36, no. 7, pp. 1279–1285.

**Li, Y.; Bao, J. L.** (2010): The relationship between autogenous shrinkage and pore structure of cement paste with mineral admixtures. *Construction and Building Materials*, vol. 24, no. 10, pp. 1855–1860.

**Li, Y. Y.; Cui, J. Z.** (2005): The multi-scale computational method for the mechanics parameters of the materials with random distribution of multi-scale grains. *Composites Science and Technology*, vol. 65, no. 9, pp. 1447–1458.

**Liu, J. X.; Zhao, Z. Y.; Deng, S. C. Liang, N. G.** (2009): A simple method to simulate shrinkage induced cracking in cement-based composites by lattice-type modeling, *Computational Mechanics*, vol. 43, no. 4, pp. 477–492.

**Liu, S; Liu, X; Guan, X. F.; He, P. F.; Yuan, Y.** (2013): A Stochastic Multi-scale Model for Predicting the Thermal Expansion Coefficient of Early-age Concrete. *CMES: Computer Modeling in Engineering and Sciences*, vol. 92, no. 2, pp. 173-191.

**Lura, P.; Jensen, O. M.** (2009): Cracking in cement paste induced by autogenous shrinkage. *Materials and Structures*, vol. 42, no. 8, pp. 1089 – 1099.

**Lura, P.; Jensen, O. M.** (2003): Autogenous shrinkage in high-performance ce-

ments paste: An evaluation of basic mechanisms. *Cement and Concrete Research*, vol. 33, no. 2, pp. 223 – 232.

**Lura, P.; Breugel, K. V.; Maruyama, I.** (2001): Effect of curing temperature and type of cement on early-age shrinkage of high-performance concrete. *Cement and Concrete Research*, vol. 31, no. 12, pp. 1867 – 1872.

**Min, K. H.; Jung, H. C.** (2010): Shrinkage characteristics of high-strength concrete for large underground space structures. *Tunneling and Underground Space Technology*, vol. 25, no. 2, pp. 108–113.

**Pichler, C.; Lackner, R.; Mang, H. A.** (2007): Multi-scale micromechanics model for the autogenous-shrinkage deformation of early-age cement-based materials. *Engineering Fracture Mechanics*, vol. 74, pp. 34–58.

**Shen, Y. B.; Xie, H. C.** (2006): A new method of controlling shrinkage cracking in repaired concrete structures using an interface layer of carbon fiber reinforced cement mortar. *CMC: Computers, Materials & Continua*, vol. 3, no. 5, pp. 49-53.

**Slowik, V.; Hübner, T.; Schmidt, M.; Villmann, B.** (2009): Simulation of capillary shrinkage cracking in cement-like materials. *Cement and Concrete Composites*, vol. 31, no. 7, pp. 461–469

**Tazawa, E.; Miyazawa, S.** (1998): Experiment study on mechanism of autogenous shrinkage of concrete. *Cement and Concrete Research*, vol. 28, no. 18, pp. 1633–1638.

**Wang, T. M.** (1997): *Crack control of engineering structures*. Beijing, Building Industry Press (in Chinese).

**Wang, Z. L.; Li, G. D.** (2013): Experimental method and prediction model for autogenous shrinkage of high performance concrete. *Construction and Building Materials*, vol. 49, pp. 400–406.

**Ye, H. L.; Tian, Y.** (2013): Influence of cracking on chloride diffusivity and moisture influential depth in concrete subjected to simulated environmental conditions. *Construction and Building Materials*, vol. 47, pp. 66–79.

**Yoo, S. W.; Kwon, S. J.; Jung, S. H.** (2012): Analysis technique for autogenous shrinkage in high performance concrete with mineral and chemical admixtures. *Construction and Building Materials*, vol. 34, pp. 1–10.

**Yu, X. G.; Cui, J. Z.** (2007): The prediction on mechanical properties of 4-step braided composites via two-scale method. *Composites Science and Technology*, vol. 67, no. 3-4, pp. 471–480.

**Zhang, J.; Hou, D.** (2012): Micromechanical modeling on autogenous and drying shrinkages of concrete. *Construction and Building Materials*, vol. 29, pp. 230–240.

**Zhang, J.; Hou, D. W.; Wei, S.** (2010): Experimental study on the relationship between shrinkage and interior humidity of concrete at early age. *Magazine of Concrete Research*, vol. 62, no. 3, pp. 191–199.

**Zhutovsky, S.; Kovler, K.; Bentur, A.** (2004): Influence of cement paste matrix properties on the autogenous curing of high-performance concrete. *Cement and Concrete Composites*, vol. 26, no. 5, pp. 499–507.